

The sensitivity of the El Niño- Indian monsoon teleconnection to Maritime Continent cold SST anomalies

Umakanth Uppara¹, Benjamin G. M. Webber¹, Manoj Joshi¹, and Turner Andrew George²

¹University of East Anglia

²University of Reading, UK

January 20, 2023

Abstract

The study investigates how sea surface temperature (SST) anomalies surrounding the Maritime Continent (MC) modulate the impact of developing El Niño events on Indian Summer Monsoon (ISM) rainfall. Using a climate model we find that the ISM rainfall response to tropical Pacific SST anomalies of eastern and central Pacific El Niño events is sensitive to the details of cold SST anomalies surrounding the MC. Furthermore, the remote rainfall responses to regions of SST anomalies do not combine linearly and depend strongly on gradients in the SST anomaly patterns. The cold SST anomalies around the MC have a significantly larger impact on the ISM response to eastern Pacific events than to central Pacific events. These results show the usefulness of idealised modelling experiments, which offer insights into the complex interactions of the ISM with modes of climate variability.

Hosted file

essoar.10512660.1.docx available at <https://authorea.com/users/578255/articles/620307-the-sensitivity-of-the-el-ni%C3%B1o-indian-monsoon-teleconnection-to-maritime-continent-cold-sst-anomalies>

1 **The sensitivity of the El Niño- Indian monsoon teleconnection to Maritime Continent cold**
2 **SST anomalies**

3

4

5 Umakanth Uppara^{1,4*}, Ben Webber¹, Manoj Joshi¹, Andrew Turner^{2,3}

6

7

8 ¹Climatic Research Unit, School of Environmental Sciences, University of East Anglia,
9 Norwich, NR4 7TJ, UK

10 ²Department of Meteorology, University of Reading, Reading, RG6 6ET, UK

11 ³National Centre for Atmospheric Sciences, University of Reading, Reading, RG6 6ES, UK

12 ⁴BK21 School of Earth Environmental Systems, Pusan National University, Busan, 46241,
13 Republic of Korea

14

15

16 *Correspondence to: umakanth@pusan.ac.kr

17

18

19

20

21

22

23

24

25 **Key points**

26

- 27 • The distribution of cold SSTs around the Maritime Continent strongly influences the Indian
28 Summer Monsoon during eastern Pacific El Niños
- 29 • The ISM response is strongly modulated by the regional meridional circulation in response
30 to changes in SST.
- 31 • Teleconnection pathways to the ISM from regions of SST anomalies combine in a non-
32 linear way.

33 **Abstract**

34

35 The study investigates how sea surface temperature (SST) anomalies surrounding the Maritime
36 Continent (MC) modulate the impact of developing El Niño events on Indian Summer Monsoon
37 (ISM) rainfall. Using a climate model we find that the ISM rainfall response to tropical Pacific
38 SST anomalies of eastern and central Pacific El Niño events is sensitive to the details of cold SST
39 anomalies surrounding the MC. Furthermore, the remote rainfall responses to regions of SST
40 anomalies do not combine linearly and depend strongly on gradients in the SST anomaly patterns.
41 The cold SST anomalies around the MC have a significantly larger impact on the ISM response to
42 eastern Pacific events than to central Pacific events. These results show the usefulness of idealised
43 modelling experiments, which offer insights into the complex interactions of the ISM with modes
44 of climate variability.

45

46

47 **Plain Language Summary**

48

49 El Niño events often coincide with droughts in the Indian subcontinent, though the correlation is
50 far from perfect, partially due to the so-called Indian Ocean Dipole (IOD). A climate model driven
51 by idealised combinations of SST anomalies is used to examine the combined influence of
52 different El Niño events and the IOD on the summer monsoon. We find that the effect of these
53 events on monsoon drought is particularly sensitive to the patterns of SST around the Maritime
54 Continent region, especially during El Niño events that occur in the far-east Pacific. These results
55 show the importance of idealised modelling experiments that can often tease apart complex
56 interactions in a way that individual state-of-the-art model runs cannot.

57

58

59

60

61

62

63

64 1. Introduction

65

66 The El Niño Southern Oscillation (ENSO) originates in the tropical Pacific Ocean, and its
67 remote influence on ISM variability and rainfall has been widely investigated, often leading to
68 droughts during the developing phase of ENSO events (Rasmusson and Carpenter, 1983; Ju and
69 Slingo, 1995; Kripalani and Kulkarni, 1997; Soman and Slingo, 1997; Webster et al., 1998). The
70 eastward shift of the Walker circulation during the developing phase of an El Niño event causes
71 anomalous subsidence of air in the Western Pacific (WP) and over the Indian subcontinent,
72 resulting in a decrease in ISM rainfall (Goswami, 1998; Kumar et al., 1999; Lau and Wang, 2006).
73 Adding to the complexity is decadal variability in the teleconnection patterns (e.g., Fan et al., 2021)
74 and the presence of different types of El Niño events: Eastern-Pacific (EP) El Niño events are
75 characterized by warm SST anomalies in the eastern equatorial Pacific, while Central-Pacific (CP)
76 events are characterized by warm SST anomalies over the central Pacific (Trenberth and Stepaniak,
77 2001; Ashok et al., 2007; Kao and Yu, 2009; Kug et al., 2009; Yeh et al., 2009). Kumar et al. (2006)
78 suggested that CP events play an important role in the ISM teleconnection, causing more severe
79 drought conditions over India than EP events.

80

81 The circulation over the WP, and the teleconnection from ENSO to the ISM, are strongly
82 influenced by SST anomalies over the Indian Ocean, and by central or eastern Pacific warm SST
83 anomalies during the developing phase of El Niño (e.g., Wang et al., 2003; Chen et al., 2007, He
84 et al., 2020). WP cooling and the associated non-linear atmospheric response is thought to be
85 important for the asymmetric duration of El Niño and La Niña events (e.g., Okumura et al., 2011).
86 It has been suggested that the presence of an IOD event (Indian Ocean Dipole, Saji et al., 1999)
87 impacts convective activity over the south-east Indian Ocean region (SEIO) and the WP during the
88 developing phase of an El Niño event (Annamalai et al., 2005) and that IOD events can reduce the
89 impact of co-occurring ENSO events on the ISM rainfall (Behera et al., 1999; Li et al., 2003; Saji
90 and Yamagata, 2003; Ashok et al., 2004; Cherchi et al., 2007; Cherchi and Navarra, 2013). Jang
91 and Straus (2012) studied the influence of adding heating/cooling over the maritime continent (MC)
92 to weaken or strengthen the ISM during the developing phase of the 1987 El Niño, showing
93 anticyclonic/cyclonic anomalies extending over India in response to MC heating/cooling,
94 respectively.

95 Despite these advances, the relationship between ENSO and the ISM is a challenging problem
96 because of the complex nature of its numerous coupled interactions. In this study an effort is made
97 to tease apart such interactions with a series of idealized model experiments using an atmosphere-
98 only General Circulation Model (GCM) forced by a range of possible SST patterns associated with
99 EP and CP El Niño types. We isolate the effects of cold SSTs across the MC on ISM rainfall during
100 the development of El Niño and study their interaction with warm SST anomalies in the central
101 and eastern Pacific. A description of the model and experiments is given in Section 2. The results
102 of the simulations are shown in Section 3, followed by discussion in Section 4 and conclusions in
103 Section 5.

104

105 **2. Methods**

106

107 The IGCM4 (Intermediate Global Circulation Model version 4; Joshi et al., 2015) used in this
108 study is a global spectral atmospheric model with a standard configuration of T42L20, i.e., $128 \times$
109 64 grid points in the horizontal and 20 layers in the vertical. This configuration of the model has
110 been used extensively in atmospheric and climate research (e.g., Joshi et al., 2015; van der Wiel
111 et al., 2016; Ratna et al., 2020, 2021). Its speed and flexibility make it well-suited for idealized
112 experiments. It has simpler parameterization schemes for physical processes such as convective
113 and boundary-layer mixing than state-of-the-art GCMs (see Joshi et al., 2015). Land surface
114 temperatures and soil moisture are allowed to evolve self-consistently with the GCM using a two-
115 layer model of the soil (Forster et al., 2000). SSTs in the control run are imposed as a seasonally
116 varying climatology (calculated over 1971-2000) of skin temperature obtained from NOAA-
117 CIRES Twentieth Century Reanalysis Version 3 (Compo et al., 2011).

118 SST anomaly composites of ENSO and IOD events are added to the control SSTs for the
119 perturbation experiments (see Text S1). A set of 10 model sensitivity experiments (listed in Table
120 1 & Table S1) are conducted by imposing SST anomalies in the Indian and Pacific Ocean basins,
121 as shown in Figure 1 & S1. The model starts from rest and is integrated for 35 years, the first five
122 years of which are discarded to account for any model spin-up. Runs “EP” and “CP” refer to the
123 full EP and CP Pacific SST anomalies respectively (Fig. 1 c-d), while subscripts “W” and “C”
124 respectively refer to runs containing only the warm (Fig. 1 a-b) or cold (Fig. S1 a-b) components
125 of the Pacific SST anomaly fields. The same subscripts are used for IOD SST anomalies, so for

126 example, EP+Ic represents the whole-basin EP SST anomalies in the Pacific, combined with the
127 cold SEIO SST anomalies associated with the IOD in the Indian Ocean (Fig. 1 e-f), while EP_C+Ic
128 represents only the cold anomalies in the EP runs, combined with cold SEIO SSTs associated with
129 the IOD (Fig. S1c-d).

130
131 In the control experiment, the model simulates ISM rainfall well, despite overestimation of
132 rainfall amounts over the northern Bay of Bengal (BoB) and the WP (Figure S2). This ISM wet
133 bias contrasts with the typical large ISM dry bias found in CMIP-class models (Sperber et al.,
134 2013). Circulation biases are consistent with these rainfall biases, e.g., low-level wind biases
135 include southerly flow across the equator over the central and eastern Indian Ocean (IO and
136 westerlies over the WP), while at the upper levels wind biases include easterly flow over the MC
137 and WP (see Figure S2).

138

139 **3. Results**

140
141 Figure 2 shows the JJAS mean rainfall and low-level 850 hPa circulation response to SST
142 anomalies in the model experiments. All runs display reductions in rainfall over the ISM and
143 enhanced rainfall (associated with cyclonic circulation anomalies) in the southern Indian Ocean
144 east of Madagascar, as well as over the Philippines. However, interesting differences do exist in
145 the magnitude and extent of these anomalies. As an example, the difference in rainfall response
146 over India between EP and EP+Ic is quite sizeable, whereas the difference in the rainfall response
147 over India between CP and CP+Ic is small. In contrast, the difference in rainfall response over
148 India between EP and EP_w is quite small, whereas the difference in the rainfall response over India
149 between CP and CP_w is larger. In addition, the cyclonic anomaly east of Madagascar is more
150 intense with larger zonal extent in CP_w compared with CP. The differences can only be in response
151 to the differences in the magnitude and the location of warming (Fig. 1a-b) as well as its spatial
152 distribution.

153

154 The atmospheric response to each set of SST forcings can be better understood by examining
155 the velocity potential and divergent winds in the upper and lower troposphere (Fig. 3 & S4). The
156 upper-level convergence (associated with anomalous subsidence) corresponding to the reduction

157 in rainfall is striking over the ISM region. In EP (Fig. 3b) there are three centres of anomalous
158 subsidence located over the Indian subcontinent, equatorial east Africa, and the Maritime
159 Continent. However, in CP (Fig. 3d) anomalous subsidence is relatively weak but appears over a
160 wider region enclosing the north Indian Ocean. When considering the warm component of the
161 SSTs only, the divergence patterns of EP_w and EP are quite similar- but those of CP_w and CP are
162 very different, with CP_w exhibiting a much stronger anomalous convergence over the western IO,
163 suggesting that the ISM response to western Pacific cold anomalies depends on whether the
164 developing El Niño is a CP or EP type.

165
166 The sensitivity of the ISM response to cold SST anomalies associated with the IOD is also
167 apparent from Figure 3. When including such anomalies, the divergence patterns in EP+Ic and
168 CP+Ic are very different to the patterns of EP and CP respectively, as is known from previous
169 work that shows the dependence of ISM response on the sign of the IOD and that IOD events can
170 reduce the impact of co-occurring ENSO events (Behera et al., 2006; Ashok et al., 2004; Shinoda
171 et al., 2004;; Lee Drbohlav et al., 2007; Cherchi and Navarra, 2013). However, our results
172 demonstrate that, for EP events, the cold SSTs in the SEIO region are sufficient to substantially
173 reduce the rainfall over India, while for CP events there is relatively little difference in the ISM
174 region. We consider possible reasons for these differences in the Discussion.

175
176 It is known that regional teleconnections from El Niño not only depend on the magnitude of
177 the SST anomalies, but also on their gradients (e.g., Trenberth and Stepaniak 2001). Accordingly,
178 we have calculated the JJAS SST gradient between Niño4 (5°S-5°N, 160°E-150°W) and the
179 northwest Pacific region (0-10°N, 130°E-150°E) as suggested by Hoell and Funk (2013), and there
180 is no significant difference in the SST gradient values in EP (0.61°C) and CP (0.59°C) respectively.
181 However, there are differences in the spatial distribution of these cold SST anomalies over WP
182 (Fig. S1a-b). Therefore, a pair of model experiments EP_C and CP_C are conducted by forcing with
183 WP cold SST anomalies alone. The ISM response is very weak in CP_C (Fig. S3a-b), which could
184 be one of the possible reasons for no significant difference between EP and EP_w. We return to the
185 potential importance of SST gradients in the Discussion.

186

187 Given the sensitivity of the model response to relatively small-scale SST anomalies, we use
188 the additional EP_{C+Ic} and CP_{C+Ic} (Fig. S1c-d) runs to investigate the degree of non-linearity in
189 the model responses to the addition of cold SST anomalies over the WP and MC regions. Fig. 4
190 shows the rainfall response to the sum of SST anomalies, compared to the sum of the rainfall
191 responses to individual SST anomalies. Fig. 4a for instance examines the difference between the
192 response in EP (Pacific basin-wide cold and warm SST anomalies) with the sum of the responses
193 in EP_W (warm anomalies only) and EP_C (cold anomalies only).

194

195 The positive rainfall anomaly over India in Fig. 4a and its further enhancement in Fig. 4c can
196 be attributed to the non-linear interactions arising from the combined SST forcing. The strong ISM
197 response in Figure 4c (well over 1 mm^d⁻¹) shows the nonlinearity in response to cold and warm
198 SST anomalies in the Pacific Ocean during a developing EP El Niño, as the reduction in ISM
199 rainfall when considering cold and warm SST anomalies separately is much lower than considering
200 the whole basin-wide SST anomaly field. In contrast, a dipole exists in ISM rainfall in Fig. 4b,
201 suggesting that during a developing CP El Niño, the response of ISM rainfall when considering
202 cold and warm SST anomalies separately is somewhat higher than considering the whole basin-
203 wide SST anomaly field. The nonlinearity is reflected in the 200 hPa anomalous wind divergence
204 pattern (Fig. S5), which shows divergent wind anomalies over large parts of Southeast Asia.

205

206 **4. Discussion**

207

208 The response to anomalous warm and cold SST forcing can be understood as a combination of
209 shifts in zonal and meridional circulation cells and equatorial Rossby waves forced by the
210 anomalous deep convection and latent heat release. The Rossby wave response is clear in Fig. 2,
211 with enhanced rainfall extending west of the dateline around 15°N and 15°S. This enhanced
212 rainfall coincides with local cold SST anomalies, emphasising that this is a remote response to the
213 central and eastern Pacific warm SSTs. In the EP_W simulations (Fig. 2a), the positive rainfall and
214 cyclonic circulation anomalies associated with this Rossby wave signal extends into southeast Asia
215 and is consistent with westerly anomalies strengthening the monsoon winds over the Bay of Bengal
216 that would create additional low-level divergence and reinforce drying over parts of India. In CP_W
217 (Fig. 2b), this enhanced rainfall is slightly further north, the low-level wind anomalies over the

218 Bay of Bengal are weaker, and the anomalies over the ISM are weaker. Therefore, there appears
219 to be a relationship between the strength of the rainfall anomalies over Southeast Asia, in turn a
220 remote Rossby wave response to the eastern Pacific warm SSTs, and the magnitude and location
221 of the dry anomalies over the Indian subcontinent.

222

223 All simulations demonstrate a clear shift in the strength and location of the Walker circulation,
224 as shown by the upper-level divergent winds and velocity potential (Fig. 3). This is stronger for
225 EP and EP_w than for CP and CP_w (compare Fig. 3 a,c with Fig. 3 b,d), which may be due to the
226 larger magnitude of the SST anomalies for EP events than CP events (Fig. 1 c,d). The upper-level
227 anomalous convergence extends from the MC region over the Bay of Bengal to the Indian
228 Subcontinent. There is also an anomalous meridional circulation cell evident over the western
229 Indian Ocean, with upper-level convergent (divergent) wind anomalies over the northern
230 (southern) IO, which form the descending (rising) branch of a local meridional overturning
231 circulation that opposes the mean circulation of the monsoon and thus contributes to the drying
232 over India (Figs. 2, 3). However, while the strength of this meridional circulation varies between
233 the experiments, it is difficult to robustly link this to the SST forcing applied.

234

235 The addition of cold SST anomalies in the SEIO region markedly reduces the magnitude of the
236 velocity potential anomalies for EP+I_C compared with EP. The rainfall anomalies for these two
237 simulations are strikingly different over the Bay of Bengal and central India, consistent with much
238 weaker wind anomalies here in EP+I_C (Fig. 2 c,e). The low-level divergent winds are also weaker
239 here (Fig. S4 c,e), likely because the low-level outflow from the reduced rainfall over the SEIO
240 counters the monsoon winds over the Bay of Bengal. As a result, the rainfall anomalies over the
241 Bay of Bengal are weaker, which may lead to further feedbacks on the regional circulation
242 anomalies. In contrast, for CP events, the enhanced rainfall over Southeast Asia is consistent with
243 stronger low-level divergent winds over the Bay of Bengal, contributing to an anomalous zonal
244 circulation cell and thus amplifying the dry anomalies over India.

245

246 The ISM response to a developing El Niño event appears to be as sensitive to the nature of
247 cold SST anomalies around the MC as it is to the actual type of El Niño event underway. For
248 example, the difference in rainfall over Southeast Asia between EP+I_C and CP+I_C may be due to

249 the meridional SST gradients around the MC, since for CP+Ic (Fig. 1f), the cooling is much more
250 pronounced to the south of the MC than to the north, while this meridional gradient is weaker for
251 EP+Ic (Fig. 1e). However, we note that the response to the cold SSTs alone (Fig. S3) is very
252 different to the response to combined warm and cold SSTs, underlining the importance of non-
253 linear combinations of local and remote responses. This non-linearity, combined with the high
254 sensitivity to small details in the SST patterns, increases the difficulty of interpreting the rainfall
255 response to individual ENSO and IOD events. Previous research has identified the high sensitivity
256 of the atmosphere to small SST perturbations over the West Pacific warm pool (Ju and Slingo,
257 1995), arising from the non-linear nature of the Clausius-Clapeyron relationship and very warm
258 climatological SSTs in the region. The responses shown above indicate that the details of the SST
259 gradients are at least as important as the location and magnitude of individual SST patterns in
260 determining the remote response, in agreement with previous studies (e.g., Hoell and Funk, 2013;
261 Karnauskas et al., 2009; Vera et al., 2004).

262
263 The IGCM experiments focussing on distinguishing the response to combinations of SST
264 patterns add new understanding to the existing knowledge on relationships between El Niño and
265 the ISM, emphasising the importance of SST anomalies and SST gradients in the vicinity of the
266 MC. Our idealised experiments necessarily include some simplifications. IGCM4 is an
267 atmosphere-only model, so there are no feedbacks from ocean-atmosphere interactions. Such
268 feedbacks are known to lead to markedly different results in coupled models compared with
269 atmosphere-only simulations (Kumar et al., 2005). Negative feedbacks from cloud-cover on SST
270 could reduce the magnitude of the tropical convection response to SST anomalies. However, using
271 an atmosphere-only model is necessary to precisely specify the SST patterns such that they
272 resemble composite anomalies, and has the benefit of avoiding the ocean biases that exist in most
273 coupled models.

275 **4. Conclusions**

276
277 We have used a simplified GCM (IGCM4) to investigate how ISM rainfall and circulation
278 respond to SST anomalies associated with EP and CP El Niño events, separated into their warm
279 and cold SST components, and in combination with cold SST components of IOD events. A key

280 result of our study is that the cold SST anomalies around the Maritime Continent strongly modulate
281 the teleconnection from warm developing El Niño SST anomalies in the central and eastern
282 Pacific. Warm Pacific SST anomalies alone do produce a strong response in the ISM region, but
283 this is strengthened and modified by the addition of the cold WP SSTs and the associated stronger
284 zonal SST gradients in a manner that is non-linear and not a simple superposition of anomalies.
285 When the Pacific warm anomalies are combined with cold SSTs anomalies around the MC (i.e.,
286 cold SSTs over WP and SEIO), the influence on the ISM rainfall and the circulation is more
287 significantly reduced in EP compared with CP El Niño events.

288
289 Differences in SST gradients create important local differences in divergence patterns that
290 induce remote responses and feedbacks. The non-linear interaction of Indian and Pacific SST
291 forcings as well as the importance of small-scale details and SST gradients in individual basins
292 hamper efforts to define a simple conceptual model of the ISM response to ENSO and the IOD.
293 The importance of accurately simulating such small-scale details presents a substantial challenge
294 for coupled ocean-atmosphere climate modelling, especially because of the complex topography
295 and island morphology in this region. Studying the individual responses of the ISM to ENSO and
296 IOD SST forcings is undoubtedly useful, but studying combinations is crucial to determining and
297 understanding the full response. Small differences in SST patterns and associated gradients can
298 have substantial impacts on ISM precipitation anomalies, which may contribute to the observed
299 variability in the ISM response to ENSO events, and as such are worthy of further research.

300

301 **Acknowledgements**

302

303 The research presented here arose from the STIMULATE project and was funded under the Met
304 Office Weather and Climate Science for Services Partnership (WCSSP) India Programme. This
305 research was carried out on the High-Performance Computing Cluster supported by the Research
306 and Specialist Computing Support service at the University of East Anglia.

307

308 **Data Availability Statement**

309 The data used in this study can be downloaded from the following websites:

310 GPCP (<https://psl.noaa.gov/data/gridded/data.gpcp.html>);
311 NOAA-CIRES V2c (https://psl.noaa.gov/data/gridded/data.20thC_ReanV2c.html)
312 IGCM used is described in Joshi et al. (2015; <https://gmd.copernicus.org/articles/8/1157/2015/>)

313 **References**

- 314 Annamalai, H., S. P. Xie, and J. P. McCreary (2005), Impact of Indian Ocean Sea surface
315 temperature on developing El Niño, *J. Clim.*, 18, 302– 319. [https://doi.org/10.1175/JCLI-](https://doi.org/10.1175/JCLI-3268.1)
316 3268.1
- 317 Ashok, K., Behera, S. K., Rao, S. A., Weng, H., & Yamagata, T. (2007). El Niño Modoki and its
318 possible teleconnection. *Journal of Geophysical Research: Oceans*, 112(11).
319 <https://doi.org/10.1029/2006JC003798>
- 320 Ashok, K., Guan, Z., Saji, N. H., & Yamagata, T. (2004). Individual and combined influences of
321 ENSO and the Indian Ocean Dipole on the Indian summer monsoon. *Journal of Climate*,
322 17(16), 3141–3155. [https://doi.org/10.1175/1520-0442\(2004\)017<3141:IACIOE>2.0.CO;2](https://doi.org/10.1175/1520-0442(2004)017<3141:IACIOE>2.0.CO;2)
- 323 Behera, S. K., Krishnan, R., & Yamagata, T. (1999). Unusual ocean-atmosphere conditions in
324 the tropical Indian Ocean during 1994. *Geophysical Research Letters*, 26(19), 3001–3004.
325 <https://doi.org/10.1029/1999GL010434>
- 326 Behera, S. K., Luo, J. J., Masson, S., Rao, S. A., Sakuma, H., & Yamagata, T. (2006). A CGCM
327 study on the interaction between IOD and ENSO. *Journal of Climate*, 19(9), 1688–1705.
328 <https://doi.org/10.1175/JCLI3797.1>
- 329 Chen, J. M., Li, T., & Shih, C. F. (2007). Fall persistence barrier of sea surface temperature in
330 the South China Sea associated with ENSO. *Journal of Climate*, 20(2), 158–172.
331 <https://doi.org/10.1175/JCLI4000.1>
- 332 Cherchi, A., & Navarra, A. (2013). Influence of ENSO and of the Indian Ocean Dipole on the
333 Indian summer monsoon variability. *Climate Dynamics*, 41(1), 81–103.
334 <https://doi.org/10.1007/s00382-012-1602-y>
- 335 Cherchi, A., Gualdi, S., Behera, S., Luo, J. J., Masson, S., Yamagata, T., & Navarra, A. (2007).
336 The influence of tropical Indian Ocean SST on the Indian summer monsoon. In *Journal of*
337 *Climate*, 20(13), 3083–3105. <https://doi.org/10.1175/JCLI4161.1>
- 338 Compo, G. P., Whitaker, J. S., Sardeshmukh, P. D., Matsui, N., Allan, R. J., Yin, X., et al.
339 (2011). The Twentieth Century Reanalysis Project. *Quarterly Journal of the Royal*
340 *Meteorological Society*, 137(654), 1–28. <https://doi.org/10.1002/qj.776>

- 341 Fan, F., Lin, R., Fang, X., Xue, F., Zheng, F., & Zhu, J. (2021). Influence of the Eastern Pacific
342 and Central Pacific Types of ENSO on the South Asian Summer Monsoon. *Advances in*
343 *Atmospheric Sciences*, 38(1), 12–28. <https://doi.org/10.1007/s00376-020-0055-1>
- 344 Forster, P. M. D. F., Blackburn, M., Glover, R., & Shine, K. P. (2000). An examination of
345 climate sensitivity for idealised climate change experiments in an intermediate general
346 circulation model. *Climate Dynamics*, 16(10–11), 833–849.
347 <https://doi.org/10.1007/s003820000083>
- 348 Goswami, B. N. (1998). Interannual variations of Indian summer monsoon in a GCM: external
349 conditions versus internal feedbacks. *Journal of Climate*, 11(4), 501–522.
350 [https://doi.org/10.1175/1520-0442\(1998\)011<0501:IVOISM>2.0.CO;2](https://doi.org/10.1175/1520-0442(1998)011<0501:IVOISM>2.0.CO;2)
- 351 He, S., Yu, J. Y., Yang, S., & Fang, S. W. (2020). ENSO's impacts on the tropical Indian and
352 Atlantic Oceans via tropical atmospheric processes: observations versus CMIP5
353 simulations. *Climate Dynamics*, 54(11), 4627–4640. [https://doi.org/10.1007/s00382-020-](https://doi.org/10.1007/s00382-020-05247-w)
354 [05247-w](https://doi.org/10.1007/s00382-020-05247-w)
- 355 Hoell, A., & Funk, C. (2013). The ENSO-related West Pacific Sea surface temperature gradient.
356 *Journal of Climate*, 26(23), 9545–9562. <https://doi.org/10.1175/JCLI-D-12-00344.1>
- 357 Jang, Y., & Straus, D. M. (2012). The Indian monsoon circulation response to El Niño diabatic
358 heating. *Journal of Climate*, 25(21), 7487–7508. [https://doi.org/10.1175/JCLI-D-11-](https://doi.org/10.1175/JCLI-D-11-00637.1)
359 [00637.1](https://doi.org/10.1175/JCLI-D-11-00637.1)
- 360 Joshi, M., Stringer, M., Van Der Wiel, K., O'Callaghan, A., & Fueglistaler, S. (2015). IGCM4:
361 A fast, parallel and flexible intermediate climate model. *Geoscientific Model Development*,
362 8(4), 1157–1167. <https://doi.org/10.5194/gmd-8-1157-2015>
- 363 Ju, J., & Slingo, J. (1995). The Asian summer monsoon and ENSO. *Quarterly Journal of the*
364 *Royal Meteorological Society*, 121(525), 1133–1168.
365 <https://doi.org/10.1002/qj.49712152509>
- 366 Kao, H. Y., & Yu, J. Y. (2009). Contrasting Eastern-Pacific and Central-Pacific types of ENSO.
367 *Journal of Climate*, 22(3), 615–632. <https://doi.org/10.1175/2008JCLI2309.1>
- 368 Karlsruh, K. B., Seager, R., Kaplan, A., Kushnir, Y., & Cane, M. A. (2009). Observed
369 strengthening of the zonal sea surface temperature gradient across the equatorial Pacific
370 Ocean. *Journal of Climate*, 22(16), 4316–4321. <https://doi.org/10.1175/2009JCLI2936.1>
- 371 Kripalani, R. H., & Kulkarni, A. (1997). Climatic impact of El Niño/La Niña on the Indian
372 monsoon: A new perspective. *Weather*, 52(2), 39–46. [https://doi.org/10.1002/j.1477-](https://doi.org/10.1002/j.1477-8696.1997.tb06267.x)
373 [8696.1997.tb06267.x](https://doi.org/10.1002/j.1477-8696.1997.tb06267.x)

- 374 Kug, J. S., Jin, F. F., & An, S. Il. (2009). Two types of El Niño events: Cold tongue El Niño and
375 warm pool El Niño. *Journal of Climate*, 22(6), 1499–1515.
376 <https://doi.org/10.1175/2008JCLI2624.1>
- 377 Kumar, K. K., Rajagopalan, B., & Cane, M. A. (1999). On the weakening relationship between
378 the Indian monsoon and ENSO. *Science*, 284(5423), 2156–2159.
379 <https://doi.org/10.1126/science.284.5423.2156>
- 380 Kumar, K. K., Hoerling, M., & Rajagopalan, B. (2005). Advancing dynamical prediction of
381 Indian monsoon rainfall. *Geophysical Research Letters*, 32,
382 L08704. <https://doi.org/10.1029/2004GL021979>
- 383 Kumar, K. K., Rajagopalan, B., Hoerling, M., Bates, G., & Cane, M. (2006). Unraveling the
384 mystery of Indian monsoon failure during El Niño. *Science*, 314(5796), 115–119.
385 <https://doi.org/10.1126/science.1131152>
- 386 Lau, N.-C., & Wang, B. (2006). Interactions between the Asian monsoon and the El
387 Niño/Southern Oscillation. In *The Asian Monsoon* (pp. 479–512). [https://doi.org/10.1007/3-](https://doi.org/10.1007/3-540-37722-0_12)
388 [540-37722-0_12](https://doi.org/10.1007/3-540-37722-0_12)
- 389 Lee Drbohlav, H. K., Gualdi, S., & Navarra, A. (2007). A diagnostic study of the Indian Ocean
390 dipole mode in El Niño and non-El Niño years. In *Journal of Climate*, 20(13), 2961–2977.
391 <https://doi.org/10.1175/JCLI4153.1>
- 392 Li, T., Wang, B., Chang, C. P., & Zhang, Y. (2003). A theory for the Indian Ocean dipole-zonal
393 mode. *Journal of the Atmospheric Sciences*, 60(17), 2119–2135.
394 [https://doi.org/10.1175/1520-0469\(2003\)060<2119:ATFTIO>2.0.CO;2](https://doi.org/10.1175/1520-0469(2003)060<2119:ATFTIO>2.0.CO;2)
- 395 Okumura, Y. M., & Deser, C. (2010). Asymmetry in the duration of El Niño and La
396 Niña. *Journal of Climate*, 23(21), 5826– 5843. <https://doi.org/10.1175/2010JCLI3592.1>
- 397 Rasmusson, E. M., & Carpenter, T. H. (1983). The relationship between eastern equatorial
398 Pacific sea surface temperatures and rainfall over India and Sri Lanka. *Monthly Weather*
399 *Review*, 111(3), 517–528. [https://doi.org/10.1175/1520-](https://doi.org/10.1175/1520-0493(1983)111<0517:TRBEEP>2.0.CO;2)
400 [0493\(1983\)111<0517:TRBEEP>2.0.CO;2](https://doi.org/10.1175/1520-0493(1983)111<0517:TRBEEP>2.0.CO;2)
- 401 Ratna, S. B., Osborn, T. J., Joshi, M., & Luterbacher, J. (2020). The influence of Atlantic
402 variability on Asian summer climate is sensitive to the pattern of the sea surface
403 temperature anomaly. *Journal of Climate*, 33(17), 7567–7590. [https://doi.org/10.1175/JCLI-](https://doi.org/10.1175/JCLI-D-20-0039.1)
404 [D-20-0039.1](https://doi.org/10.1175/JCLI-D-20-0039.1)
- 405 Ratna, S. B., Cherchi, A., Osborn, T. J., Joshi, M., & Uppara, U. (2021). The Extreme Positive
406 Indian Ocean Dipole of 2019 and Associated Indian Summer Monsoon Rainfall Response.
407 *Geophysical Research Letters*, 48(2). <https://doi.org/10.1029/2020GL091497>

- 408 Saji, N. H., Goswami, B. N., Vinayachandran, P. N., & Yamagata, T. (1999). A dipole mode in
409 the tropical Indian Ocean. *Nature*, 401(6751), 360–363. <https://doi.org/10.1038/43854>
- 410 Saji, N. H., & Yamagata, T. (2003). Structure of SST and surface wind variability during Indian
411 Ocean Dipole mode events: COADS observations. *Journal of Climate*, 16(16), 2735–2751.
412 [https://doi.org/10.1175/1520-0442\(2003\)016<2735:SOSASW>2.0.CO;2](https://doi.org/10.1175/1520-0442(2003)016<2735:SOSASW>2.0.CO;2)
- 413 Shinoda, T., Alexander, M. A., & Hendon, H. H. (2004). Remote response of the Indian Ocean
414 to interannual SST variations in the tropical Pacific. *Journal of Climate*, 17(2), 362–372.
415 [https://doi.org/10.1175/1520-0442\(2004\)017<0362:RROTIO>2.0.CO;2](https://doi.org/10.1175/1520-0442(2004)017<0362:RROTIO>2.0.CO;2)
- 416 Soman, M. K., & Slingo, J. (1997). Sensitivity of the Asian summer monsoon to aspects of sea-
417 surface-temperature anomalies in the tropical Pacific Ocean. *Quarterly Journal of the Royal*
418 *Meteorological Society*, 123(538), 309–336. <https://doi.org/10.1256/smsqj.53803>
- 419 Sperber, K. R., Annamalai, H., Kang, I. S., Kitoh, A., Moise, A., Turner, A., et al. (2013). The
420 Asian summer monsoon: An intercomparison of CMIP5 vs. CMIP3 simulations of the late
421 20th century. *Climate Dynamics*, 41(9–10), 2711–2744. [https://doi.org/10.1007/s00382-](https://doi.org/10.1007/s00382-012-1607-6)
422 [012-1607-6](https://doi.org/10.1007/s00382-012-1607-6)
- 423 Trenberth, K. E., & Stepaniak, D. P. (2001). Indices of El Niño evolution. *Journal of Climate*,
424 14(8), 1697–1701. [https://doi.org/10.1175/1520-0442\(2001\)014<1697:LIOENO>2.0.CO;2](https://doi.org/10.1175/1520-0442(2001)014<1697:LIOENO>2.0.CO;2)
- 425 van der Wiel, K., Matthews, A. J., Joshi, M. M., & Stevens, D. P. (2016). The influence of
426 diabatic heating in the South Pacific Convergence Zone on Rossby wave propagation and
427 the mean flow. *Quarterly Journal of the Royal Meteorological Society*, 142(695), 901–910.
428 <https://doi.org/10.1002/qj.2692>
- 429 Vera, C., Silvestri, G., Barros, V., & Carril, A. (2004). Differences in El Niño response over the
430 Southern Hemisphere. *Journal of Climate*, 17(9), 1741–1753. [https://doi.org/10.1175/1520-](https://doi.org/10.1175/1520-0442(2004)017<1741:DIENRO>2.0.CO;2)
431 [0442\(2004\)017<1741:DIENRO>2.0.CO;2](https://doi.org/10.1175/1520-0442(2004)017<1741:DIENRO>2.0.CO;2)
- 432 Wang, B., Wu, R., & Li, T. (2003). Atmosphere-warm ocean interaction and its impacts on
433 Asian-Australian monsoon variation. *Journal of Climate*, 16(8), 1195–1211.
434 [https://doi.org/10.1175/1520-0442\(2003\)16<1195:AOIAII>2.0.CO;2](https://doi.org/10.1175/1520-0442(2003)16<1195:AOIAII>2.0.CO;2)
- 435 Webster, P. J., Magaña, V. O., Palmer, T. N., Shukla, J., Tomas, R. A., Yanai, M., & Yasunari,
436 T. (1998). Monsoons: processes, predictability, and the prospects for prediction. *Journal of*
437 *Geophysical Research: Oceans*, 103(C7), 14451–14510. <https://doi.org/10.1029/97jc02719>
- 438 Yeh, S. W., Kug, J. S., Dewitte, B., Kwon, M. H., Kirtman, B. P., & Jin, F. F. (2009). El Niño in
439 a changing climate. *Nature*, 461(7263), 511–514. <https://doi.org/10.1038/nature08316>

440

441

442

443 **Figures**

444 **Figure 1.** The JJAS mean composites of SST anomalies overlaid with SST climatology to provide
445 surface forcing in IGCM model experiments for EP, CP. In our naming convention, EP and CP
446 suggest whole Pacific-basin SST anomalies, while W and C subscripts indicate experiments in
447 which only the warm or cold SST anomalies are retained (respectively) for El Niño (over Pacific
448 Ocean) and IOD (over Indian Ocean) events.

449

450 **Figure 2.** IGCM responses in JJAS rainfall (shaded, mm d^{-1}) and circulation (850 hPa wind
451 vectors; m s^{-1}) over the ISM domain for the 6 model experiments shown in Figure 1. **(a-b)** the
452 model response to Pacific warm SST forcing only (EP_w , CP_w); **(c-d)** model response to whole-
453 basin SST forcing (EP, CP); **(e-f)** model response to EP, CP SSTs combined with cold Indian
454 Ocean SST anomalies associated with IOD events ($\text{EP}+\text{I}_c$, $\text{CP}+\text{I}_c$). The wind vectors (black) and
455 the precipitation (hatched) represent statistical significance at the 90% confidence level based on
456 a student's t-test.

457

458 **Figure 3.** Same as Figure 2, but for upper level (200 hPa) velocity potential (shaded; 10^{-6} , $\text{m}^2 \text{s}^{-1}$)
459 overlaid with divergent wind anomalies (vectors). Only signals of velocity potential significant at
460 the 90% level are shown (shaded), while divergent winds are shaded grey (black) below (above)
461 this level.

462

463 **Figure 4.** Non-linearity in IGCM responses to SST forcing during JJAS, (a-b) rainfall (shaded,
464 mm d^{-1}) and circulation (850 hPa wind vectors; m s^{-1}) responses between EP (CP) and the sum of
465 responses to EP_w and EP_c (CP_w and CP_c), (c-d) between $\text{EP}+\text{I}_c$ ($\text{CP}+\text{I}_c$) and the sum of responses
466 to EP_w and EP_c+I_c (CP_w and CP_c+I_c).

467

468 **Tables**

469

470 **Table 1:** The list of model experiments. In our naming convention, EP and CP suggest whole
471 Pacific basin SST anomalies, while 'W' and 'C' subscripts indicate experiments where only the

472 warm or cold SST anomalies are retained (respectively) for El Niño (over Pacific Ocean) and IOD
473 (over Indian Ocean) events.

474

475

476

477

478

479

480

481

482

483

484

485

486

487

488

489

490

491

492

493

494

495

496

497

498

499

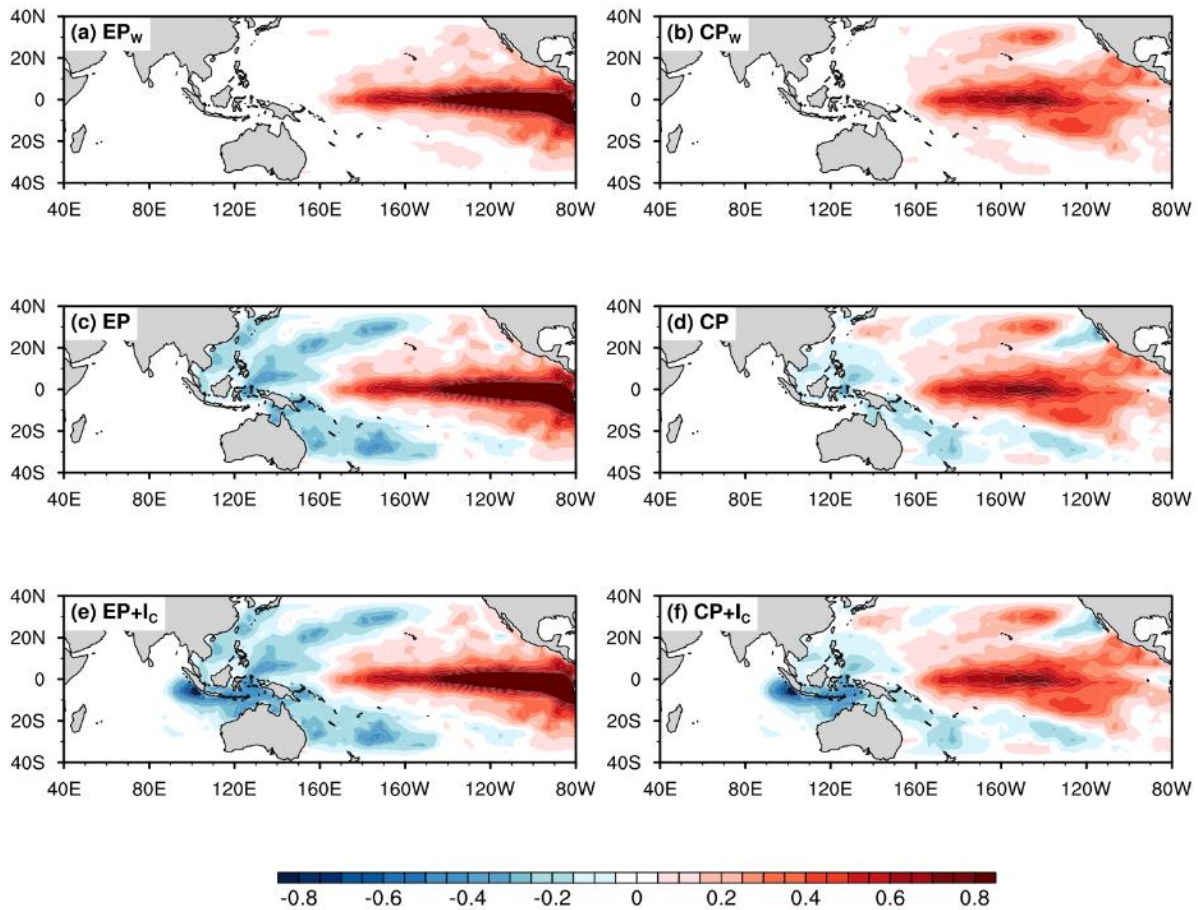
500

501

502

503 **Figures**

504



505

506

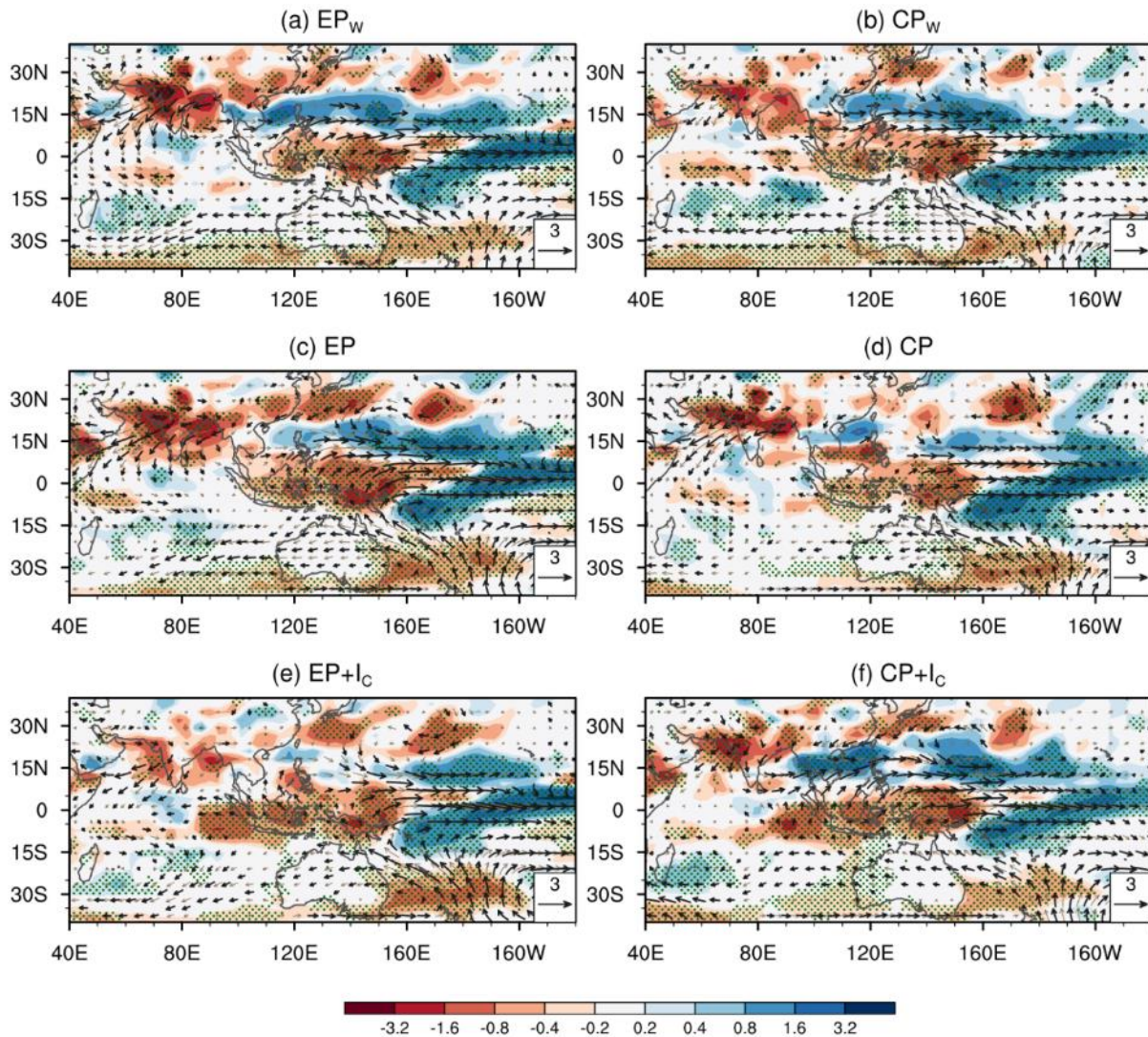
507 **Figure 1.** The JJAS mean composites of SST anomalies overlaid with SST climatology to provide
508 surface forcing in IGCM model experiments for EP, CP. In our naming convention, EP and CP
509 suggest whole Pacific-basin SST anomalies, while W and C subscripts indicate experiments in
510 which only the warm or cold SST anomalies are retained (respectively) for El Niño (over Pacific
511 Ocean) and IOD (over Indian Ocean) events.

512

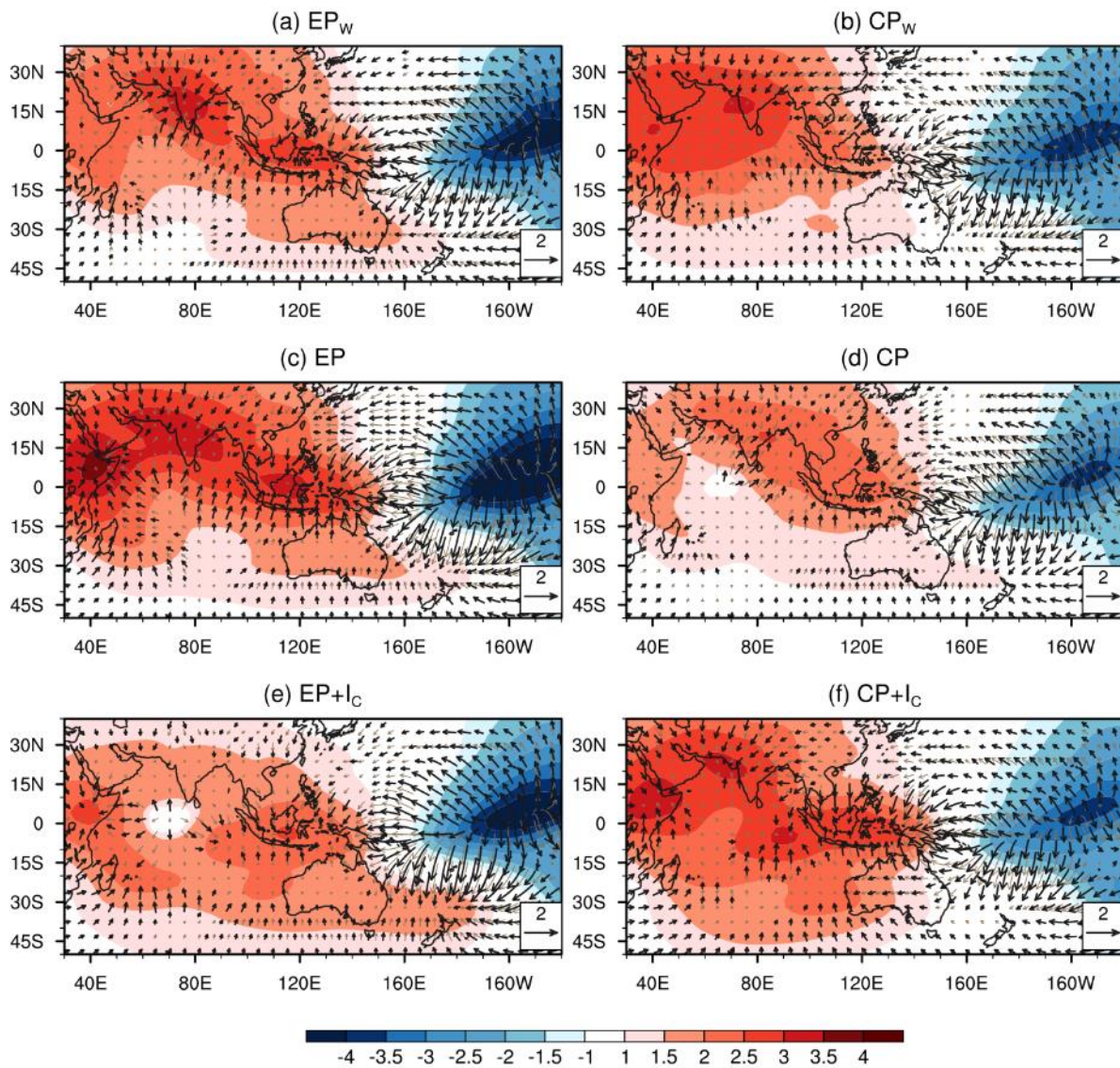
513

514

515



516
 517
 518 **Figure 2.** IGCM responses in JJAS rainfall (shaded, mm d^{-1}) and circulation (850 hPa wind
 519 vectors; m s^{-1}) over the ISM domain for the 6 model experiments shown in Figure 1. **(a-b)** the
 520 model response to Pacific warm SST forcing only (EP_w , CP_w); **(c-d)** model response to whole-
 521 basin SST forcing (EP, CP); **(e-f)** model response to EP, CP SSTs combined with cold Indian
 522 Ocean SST anomalies associated with IOD events ($\text{EP}+\text{I}_c$, $\text{CP}+\text{I}_c$). The wind vectors (black) and
 523 the precipitation (hatched) represent statistical significance at the 90% confidence level based on
 524 a student's t-test.
 525
 526



528

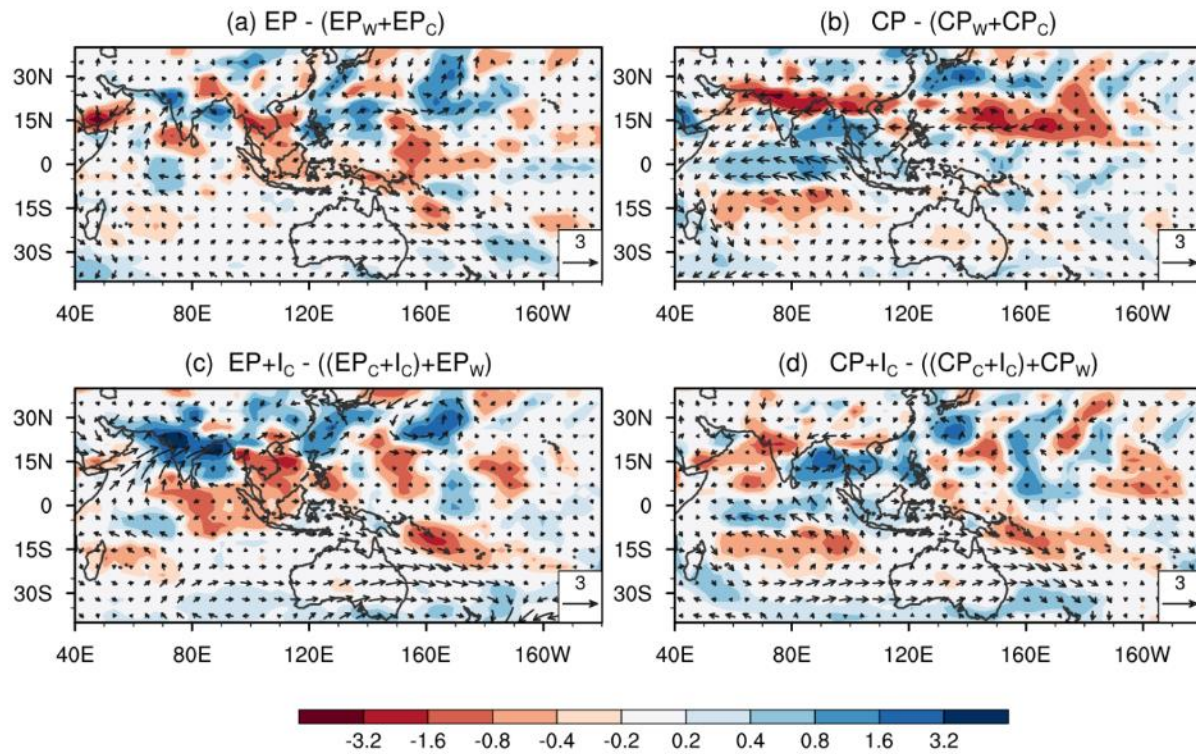
529 **Figure 3.** Same as Figure 2, but for upper level (200 hPa) velocity potential (shaded; 10^{-6} , $m^2 s^{-1}$)
 530 overlaid with divergent wind anomalies (vectors). Only signals of velocity potential significant at
 531 the 90% level are shown (shaded), while divergent winds are shaded grey (black) below (above)
 532 this level.

533

534

535

536



538

539 **Figure 4.** Non-linearity in IGCM responses to SST forcing during JJAS, (a-b) rainfall (shaded,
 540 mm d⁻¹) and circulation (850 hPa wind vectors; m s⁻¹) responses between EP (CP) and the sum of
 541 responses to EP_W and EP_C (CP_W and CP_C), (c-d) between EP+I_C (CP+I_C) and the sum of responses
 542 to EP_W and EP_C+I_C (CP_W and CP_C+I_C).

543

544

545

546

547

548

549

550

551

552

553

554 **Tables**

555

556 **Table 1:** The list of model experiments. In our naming convention, EP and CP suggest whole
557 Pacific basin SST anomalies, while ‘W’ and ‘C’ subscripts indicate experiments where only the
558 warm or cold SST anomalies are retained (respectively) for El Niño (over Pacific Ocean) and IOD
559 (over Indian Ocean) events.

560

Experiments	SST forcing
Control (Ctrl)	Monthly SST climatology
EP _w , CP _w	Ctrl + Pacific Warm SST anomalies
EP, CP	Ctrl + Pacific Basin SST anomalies
EP+I _c , CP+I _c	Ctrl + Pacific Basin + IOD Cold SST anomalies

561

562

The sensitivity of the El Niño- Indian monsoon teleconnection to Maritime Continent cold SST anomalies

Umakanth Uppara^{1*}, Ben Webber¹, Manoj Joshi¹, Andrew Turner^{2,3}

¹Climatic Research Unit, School of Environmental Sciences, University of East Anglia,
Norwich, NR4 7TJ, UK

²Department of Meteorology, University of Reading, Reading, RG6 6ET, UK

³National Centre for Atmospheric Sciences, University of Reading, Reading, RG6 6ES,
UK

*Correspondence to: u.uppara@uea.ac.uk

Contents of this file

Text S1

Figures S1 to S5

Table S1

Text S1

The developing years of composites of EP are 1951, 1969, 1972, 1976, 1982, 1987, 1997, 2006 and the CP are 1953, 1957, 1963, 1965, 1968, 1977, 1991, 1994, 2002, 2004, 2009 and the positive IOD years are 1961, 1963, 1972, 1982, 1983, 1994, 1997, 2006, 2012, 2015 respectively. The Pacific anomalies for the developing phase of an El Niño year (0) are derived by compositing SST anomalies from November of year (-1) to October of year (0). October-November is chosen as the best month to transition between year 0 and year -1 to minimise the impact of any shock on the monsoon season. The developing ENSO period typically has SST anomalies during the Indian Monsoon season in JJAS of year (0), which have a strong influence on concurrent ISM rainfall and circulation (e.g., Wang et al., 2003; Jang and Straus, 2012).

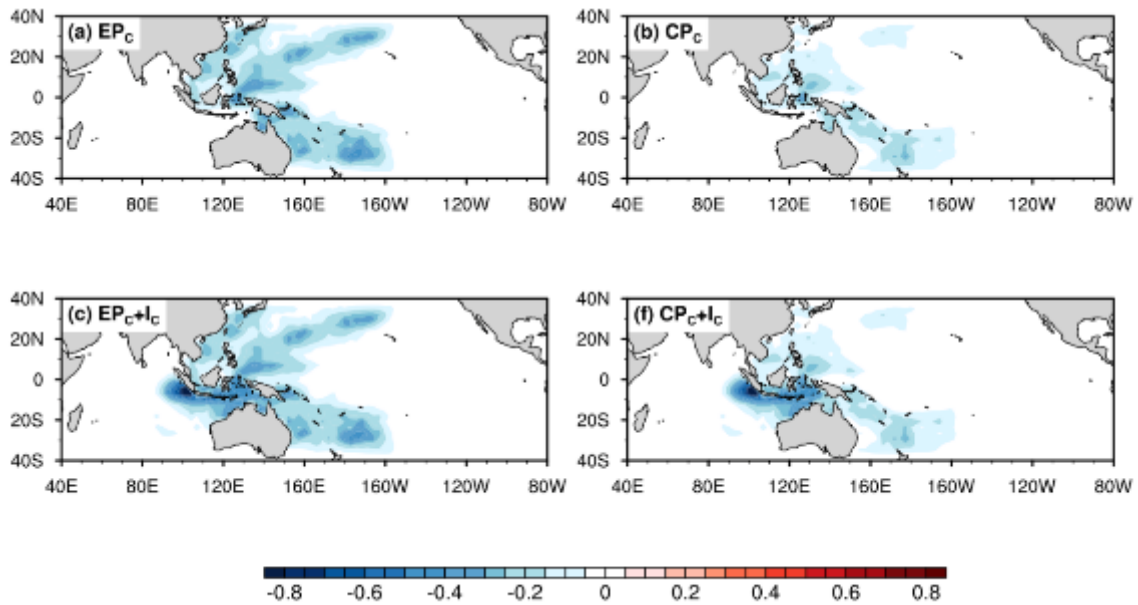


Figure S1. The JJAS mean composites of SST anomalies overlaid with SST climatology to provide surface forcing in IGCM model experiments for EP, CP. In our naming convention, EP and CP suggest whole Pacific-basin SST anomalies, while W and C subscripts indicate experiments in which only the warm or cold SST anomalies are retained (respectively) for El Niño (over Pacific Ocean) and IOD (over Indian Ocean) events.

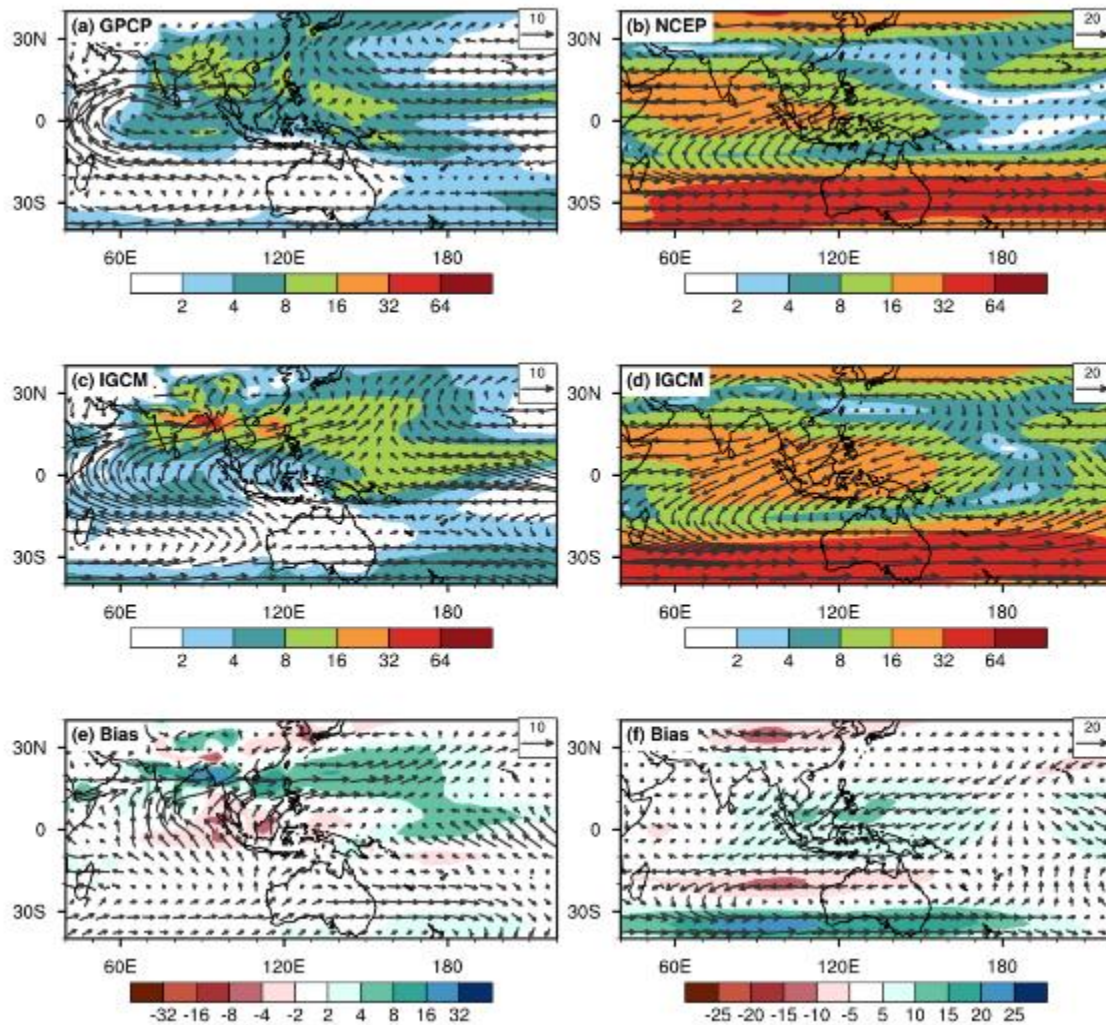


Figure S2. Observed (reanalysis) and IGCM-simulated climatology of JJAS rainfall (mm d^{-1}) and the circulation (wind vector, m s^{-1}). **(a)** GPCP rainfall (contours) overlaid with 850 hPa winds (NCEP), **(b)** 200 hPa winds speed (shaded) overlaid with wind vectors. **(c & d)** represents the IGCM-simulated rainfall and circulation, and **(e & f)** indicate the model biases. The climatology in reanalysis is based on the period 1979-2008, while the IGCM climatology is based on the years after the model spin up (in this case 30 years)

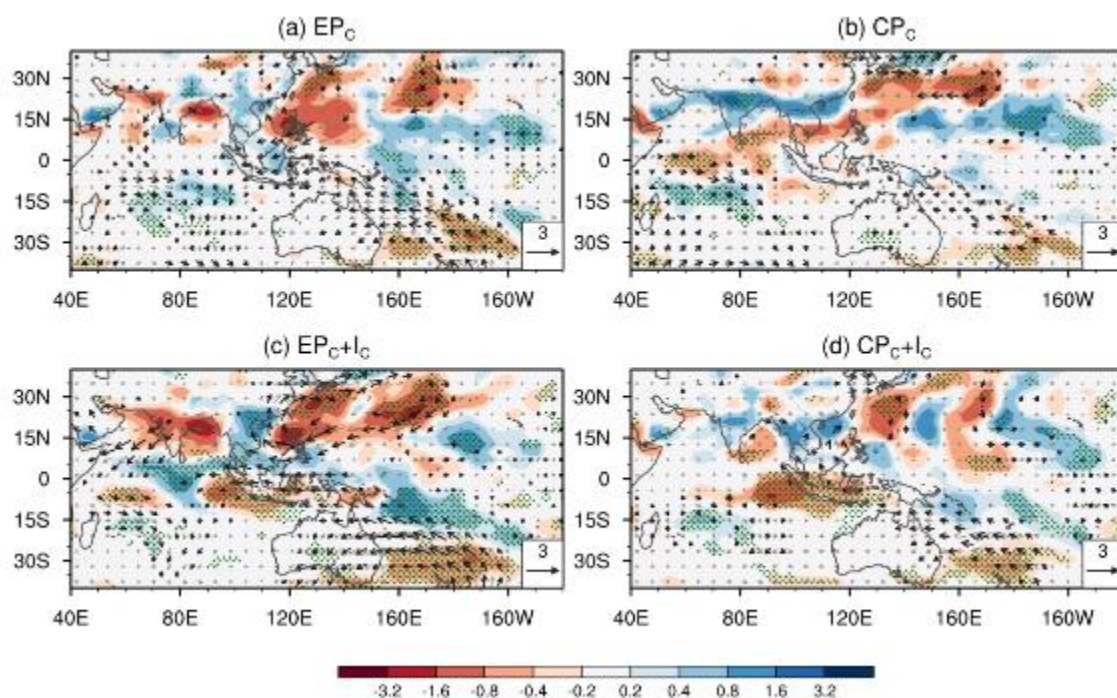


Figure S3. IGCM responses in JJAS rainfall (shaded, mm d^{-1}) and circulation (850 hPa wind vectors; m s^{-1}) over the ISM domain for the 4 model experiments shown in Figure 1. **(a-b)** the model response to Pacific cold SST forcing only (EP_C , CP_C); **(c-d)** model response to Pacific cold SSTs combined with cold Indian Ocean SST anomalies (I_C). The wind vectors (black) and the precipitation (hatched) represent statistical significance at the 90% confidence level based on a student's t-test.

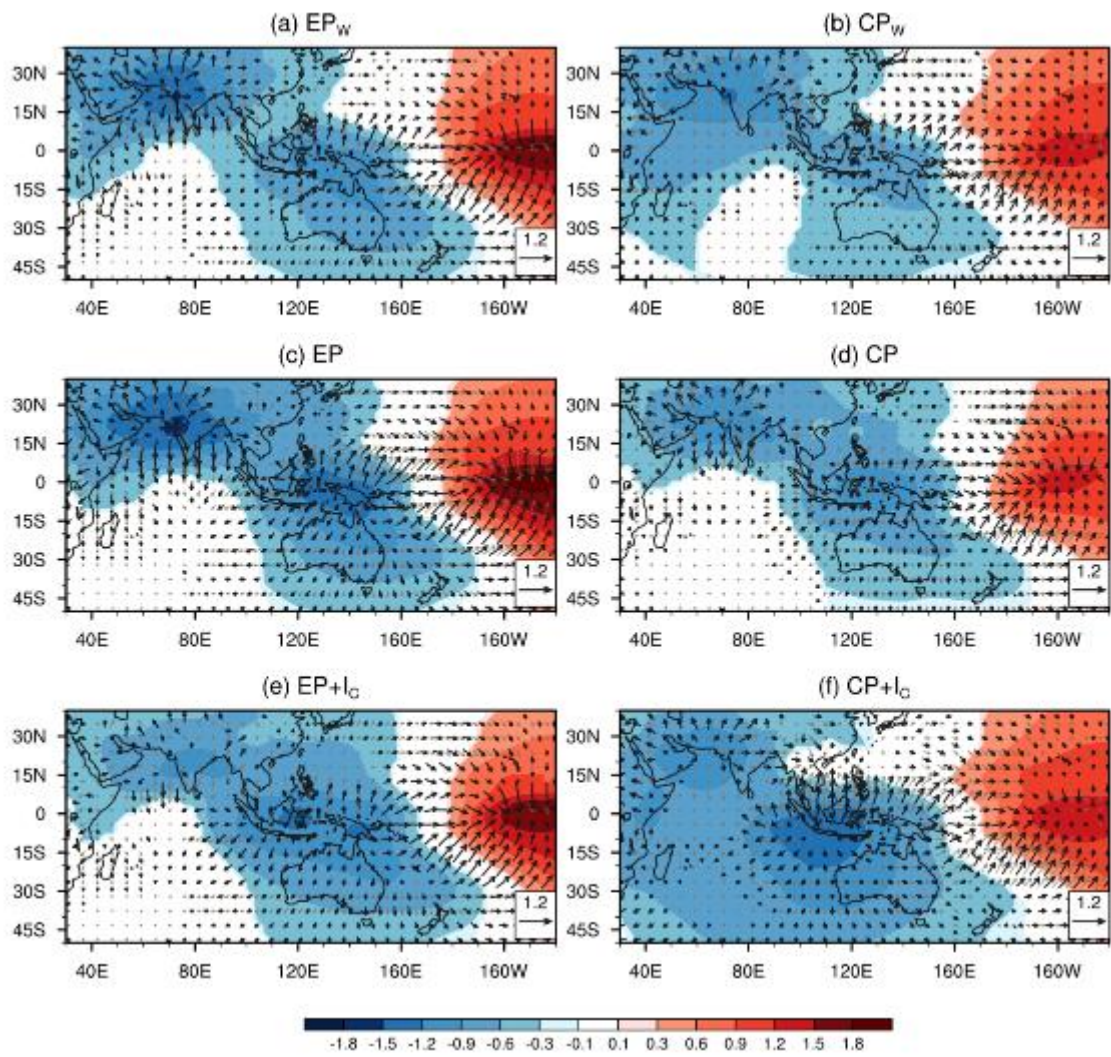


Figure S4. Same as Figure 2, but for lower level (850 hPa) velocity potential (shaded; 10^6 , $m^2 s^{-1}$) overlaid with divergent wind anomalies (vectors). Only signals of velocity potential significant at the 90% level are shown (shaded), while divergent winds are shaded grey (black) below (above) this level.

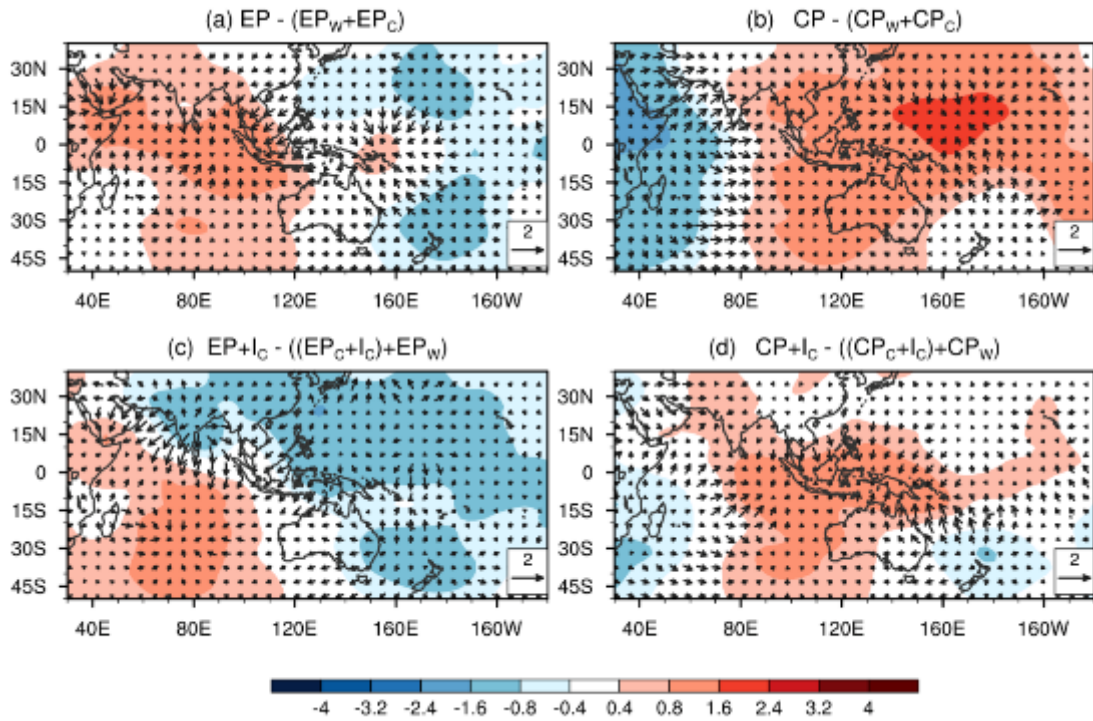


Figure S5. Non-linearity in IGCM responses to SST forcing during JJAS, (a-b) upper-level (200 hPa) velocity potential (shaded; $10^{-6} \text{ m}^2 \text{ s}^{-1}$) overlaid with divergent wind anomalies (vectors) between EP (CP) and the sum of responses to EP_w and EP_c (CP_w and CP_c), (c-d) between $EP + I_c$ ($CP + I_c$) and the sum of responses to EP_w and $EP_c + I_c$ (CP_w and $CP_c + I_c$).

Tables

Table S1: Additional model experiments. In our naming convention, EP and CP suggest whole Pacific basin SST anomalies, while W and C subscripts indicate experiments where only the warm or cold SST anomalies are retained (respectively) for El Niño (over Pacific Ocean) and IOD (over Indian Ocean) events.

Experiments	SST forcing
EP _C , CP _C	Ctrl + Pacific cold SST anomalies
EP _C +I _C , CP _C +I _C	Ctrl + Pacific cold + IOD cold SST anomalies